HOKKAIDO UNIVERSITY

Title	Multilayered MoS2 nanoflakes bound to carbon nanotubes as electron acceptors in bulk heterojunction inverted organic solar cells
Author(s)	Jeon, Il; Kutsuzawa, Dai; Hashimoto, Yu et al.
Citation	Organic Electronics, 17, 275-280 https://doi.org/10.1016/j.orgel.2014.12.025
Issue Date	2015-02
Doc URL	https://hdl.handle.net/2115/58440
Type	journal article
File Information	ORGELE-D-14-00870 revised MS.pdf



Hokkaido University Collection of Scholarly and Academic Papers : HUSCAP

Multilayered MoS_2 Nanoflakes Bound to Carbon Nanotubes as Electron Acceptors in Bulk Heterojunction Inverted Organic Solar Cells

Il Jeon[1] Dai Kutsuzawa[2] Yu Hashimoto[2] Takashi Yanase[2] Taro Nagahama[2] Toshihiro Shimada[2,*] and Yutaka Matsuo[1,*]

1 Department of Chemistry, School of Science, The University of Tokyo, 7-3-1 Hongo, Bunkyo-ku, Tokyo 113-0033, Japan

2 Division of Materials Chemistry, Faculty of Engineering, Hokkaido University, Kita-ku, Sapporo 060-8628, Japan

Correspondence to matsuo@chem.s.u-tokyo.ac.jp (Y. Matsuo) and shimadat@eng.hokudai.ac.jp (T. Shimada)

Abstract: We demonstrate the deposition of multilayered MoS_2 on a low-cost metallic-semiconducting carbon nanotube via chemical vapor deposition, and the use of this material as electron acceptor species forming a bulk heterojunction with P3HT in inverted-type organic photovoltaics (OPVs). This is an uplifting discovery, in which MoS_2 has been used as an electron acceptor in spite of its innate immiscibility with organic compounds. This is possible because we utilize carbon nantube's nature to intercalate with P3HT through π-π interaction. The successful binding of MoS_2 onto carbon nanotube bundles and its optoelectronic effect as a photovoltaic device has been lucidly analyzed through various techniques in this paper. The effect has been ultimately evidenced by a power conversion efficiency of 0.46%, which proves MoS_2 with many advantages can also be used as a photoactive layer.

Keywords: Carbon Nanotubes, Molybdenum Disulfides, Chemical Vapor Deposition, Electron Acceptors, Photovoltaics

1. Introduction

Research in organic-inorganic hybrid solar cells continues to rise in recent years.[1] It is well known that organic acceptors have drawbacks in low stability and mobility, whereas inorganic materials have advantages in both stability and charge carrier mobility. Furthermore, by controlling its size, a wide range of band gap configuration can be achieved. Among the inorganic materials, layered n-type semiconductors have widely been studied for photovoltaic applications.[2-6] Such crystalline semiconductors have wave functions as loosely bound valence electrons overlapping each other to form a global conduction band. Carriers can freely travel through the extended states.[7] However, in organic materials, the charge carriers tend to be localized in potential wells consisting of single molecules or conjugated molecular segments. Carriers hop between these energy states through vibrations of host and adjacent molecules. These hopping is less efficient than propagating through an extended conduction band, which causes organic materials to have a lower carrier mobility.[8, 9] As a layered n-type semiconductor, transition metal dichalcogenides have recently been drawing attention. With a formula MX_2, where M is a transition metal element from group VI (Mo and W), strong in-plane bonding and weak out-of-plane interactions allow us to control its two-dimensional layer thickness.[10] Amid a variety of constituent elements, we have grown MoS_2 multilayered nanoflakes for its apt workfunction value of 4.8 eV which is very close to the Fermi level of CNTs and we know that since their Fermi levels are similar, there is no doping effect[11,12] MoS_2 with its quality of being easily grafted onto CNTs using a chemical vapor deposition (CVD) makes it an outstanding candidate for this enables intercalation with other organic materials like P3HT.[24-27] Moreover MoS_2 has no charge traps due to the absence of dangling bonds on its surface, and has easily tunable optical band gap by controlling the layer number. Also, MoS_2 multilayer has a higher mobility of 50-200 $cm^2V^{-1}s^{-1}$ than its monolayer counterpart with a mobility of 1-8 $cm^2V^{-1}s^{-1}$.[13-23] Despite such advantages, multilayered MoS_2 has not been reported as photoactive materials in bulk heterojunction (BHJ) systems. There are mainly two reasons: one is that in the case of MoS_2,

there is no interaction between MoS_2 and P3HT. With such immiscibility, BHJ is not possible. In a BHJ, electron donor and acceptor should be thoroughly mixed for efficient exciton separations to occur. The device performance is heavily dependent on the degree of dispersion and the interfacial area. Second reason is that the multilayered MoS_2 is more difficult to produce than the single-layered compound due to difficulties in thickness control. [24,25] Therefore, we show in this paper, a novel methodology of introducing MoS_2 multilayer into an OSC BHJ system through an atmospheric CVD using MoO_3 and S as sources, and unsorted single wall carbon nanotubes (SWCNTs) on a metal chip as a substrate.[26,27] The unpurified semiconducting-and-metallic mixed SWCNTs are inexpensive materials that can assist the intercalation of MoS_2 with P3HT. P3HT can provide isolation between the CNTs, thus minimizing the direct electronic coupling between the optically active semiconducting nanotubes and the metallic nanotubes present in the mixture (at approximately 30 wt %) that may quench the photo-generated excitons.[28] Using the MoS_2CNT, we fabricated an inverted type OSC rather than a normal structure for its high stability, air-processability, and its facile process.[29] We obtain a power conversion efficiency (PCE) of 0.46%, while a costly and highly pure semiconducting SWCNT and P3HT based OSC has given PCE of 0.72%[30] This is an encouraging result for we achieve a PCE as good as the expensive semiconducting SWCNT based device using the unpurified SWCNTs.

2. Material and methods

2.1 Deposition of multilayered MoS_2 nanoflakes on CNT bundle

Multilayered MoS_2 nanoflakes were deposited on CNT (Hipco) bundles by a CVD. (Fig. 1). S powder (99.5%, Kanto Chemical) was placed in a quartz tube, MoO_3 powder (99.5%, Kanto Chemicals) was placed on an alumina boat in Zone 1 and Zone 2. One spatula spoonful of CNTs (0.3 mg) on a SiO_2/Si substrate (SiO_2 : 1 × 1 cm^2, 285 nm thick) was placed on a boat in Zone 3. The vapors of S and MoO_3 were introduced through N_2 flows (99.99%) labeled as

Flow 1 and Flow 2. Firstly, Flow 1 was introduced at the rate of 850 sccm and the temperature of Zone 2 and Zone 3 were increased to 650°C (r.t. to 450°C in 3 hrs and 30 minutes, and then 450°C to 650°C in 30 minutes) and 850°C (r.t. to 700°C in 3 hrs and 30 minutes, and then 700°C to 850°C in 30 minutes) each. Then, 3 hr 20 minutes after the Flow 1 was introduced, the temperature of Zone 1 was increased to 250°C in 10 minutes. After the temperatures of Zone 2 and Zone 3 reached 650°C and 850°C, N_2 Flow 2 was introduced at the rate of 360 sccm. 4 hrs later, Flow 2 was immediately turned off and the temperature of all zone were cooled to r. t. with Flow 1 maintained at the rate of 50 sccm. Product formed on a SiO_2 substrate was put into a vial containing ethanol, which separated our product from the substrate. The substrate and ethanol were later removed.

2.2 P3HT and MoS_2CNT Active layer preparation

P3HT:MoS_2CNT devices were fabricated in the following manner. A poly(3-hexylthiophene) (P3HT, regioregular, Sigma Aldrich Chemical Co., Inc.) 20 mg/mL in ortho-dichlorobenzene (ODCB, anhydrous, 99%, Sigma Aldrich Chemical Co., Inc.) and MoS_2CNTs flakes dissolved in ODCB in concentration of 5 mg/mL were prepared. In case aggregation of CNT were visible, we sonicated MoS_2CNT for less than 10 min before mixing P3HT. The composition of the active layer was produced by mixing together the two solutions in different proportion under stirring to achieve a solution of P3HT/MoS_2CNT with MoS_2CNT having a concentration of 3 wt%. The resulting solution, containing P3HT/MoS_2CNT nanofilaments, showed aggregation after 1 hr, therefore, we advice to use the solution directly into the fabrication.

2.3 Device Fabrication

ITO substrates (22 × 38 mm^2) with a sheet resistance of 6 Ω/square (Kuramoto Co., Ltd.) were first etched using Zn and 1M HCl, followed by sonicating the substrates sequentially in cleaning surfactant (Semi Clean, M-Lo), water, acetone and 2-isopropanol for 15 minutes each. The substrates were then dried in an oven at 70 °C. Prior to ZnO deposition, ITO

substrates were exposed to UV/O_3 for 30 min. The ZnO sol-gel films were prepared using the method reported by Heeger and co-workers.[31] A 0.1 M solution of zinc acetate dihydrate [$Zn(CH_3COO)\ 2H_2O$] (Wako, 99.0%) in ethanol (Wako, 99.5%) was prepared and then subjected to rigorous stirring for 2–3 h at 80 °C. Next, an ethanolamine stabilizer (28% in weight) was added and the solution was left stirring for a further 12-15 h at 60 °C. Prepared ZnO sol-gel solution was then deposited onto ITO substrates through a cellulose acetate filter (0.45 μm pore size) by spin coating at a spin speed of 3000 rpm for 45 seconds. Next the samples were annealed at 200 ºC for 1 hr.

The P3HT/MoS_2CNT solution was then spin-coated on the ZnO layers at a speed of 850 rpm for 45 sec to give films of approximately 300 nm. The films were then immediately placed in a petri-dish for 40 minutes to allow slow evaporation of the solvent. A poly-(3,4-ethylenedioxythiophene)-polystyrenesulfonic acid (PEDOT:PSS) dispersion in water (Clevios P VP, Heraeus Precious Metals GmbH & Co.) containing 0.5 wt% polyoxyethylene(6) tridecyl ether (Sigma Aldrich Chemical Co., Inc.) was spin-coated on top of the active layer to form the hole transport layer with a 30 nm thickness. An approximately 200 nm thick Au layer was thermally evaporated at pressure of 3 x 10^{-3} Pa, with the use of a shadow mask, which defined the device active area as 1 cm^2. All processes, except for Au deposition, were performed in air and the devices were not encapsulated.

2.4 Photovoltaic Characterization

Current–voltage (J–V) characteristics were measured using a software-controlled source meter (Keithley 2400) under dark conditions and 1 Sun AM 1.5 G simulated sunlight irradiation (100 mW cm^{-2}) using a solar simulator (EMS-35AAA, Ushio Spax Inc.), which was calibrated using a silicon diode (BS-520BK) Resistance of solar cells was measured by reading a gradient off the J-V curve. As resistance equals to voltage over current, the series resistance was taken from the slope of the graph at the open-circuit voltage. And the shunt resistance was taken from the slope of the graph near the short-circuit current point.

2.5 MoS_2 on CNT Characterizations

The morphology of MoS_2CNTs was observed by transparent electron microscope (TEM; JEOL JEM-2010) and the number of layers of deposited MoS_2 was estimated by Raman microscope with a ×50 lens and 5×10^{-6} % of 200 mW power (Renishaw InVia with 532 nm excitation). Elemental analysis was shown by auger electron microscope (AES; JEOL).

2.6 Other Characterizations

UV-vis absorption spectra were measured on JASCO V-670 spectrometer (Nihon bunko). Photoluminescence was measured using JASCO FP6500 spectrophotometer; at room temperature (298 K) in a 1 x 1 cm glass substrate. Excitation wavelength of 400 nm was used.

3. Results and Discussion

Firstly, For the multilayer generation and the control of layer number, we use two separate furnaces which introduce S and MoO_3 at different rates and temperatures.[23-26] (Figure 1)

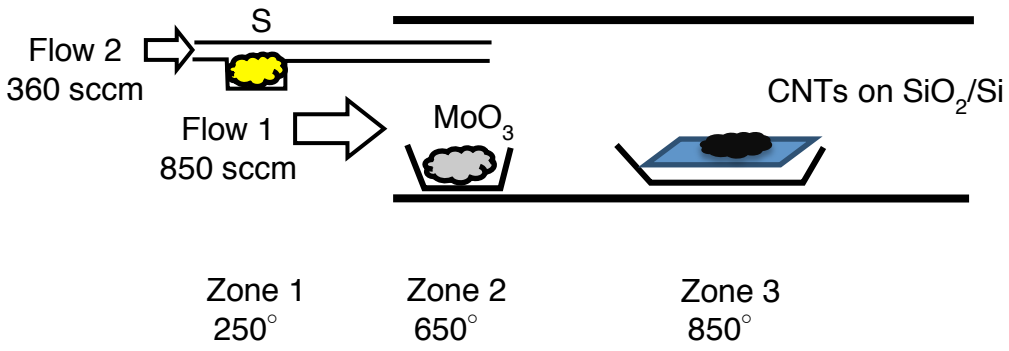


Figure 1. Illustration of the CVD for the multilayered MoS_2 nanoflakes

As well as having a higher mobility, multilayered MoS_2 is known to have an indirect band gap of 1.2 eV, which we think is more favorable than its monolayer counterpart in terms of its energy band alignment.[32] With decrease in crystal thickness, the band gap widens and reaches 1.8 eV for the monolayer which has a direct energy gap[33]. Through this method, we have deposited multilayered MoS_2 on bundles of carbon nanotube (CNT). Successful

deposition has been shown by transmission electron microscopy (TEM). (Figure 2) For CNT, the difference is clear and we can observe MoS_2 flakes from the after-deposition image. (Figure 2 a) b))

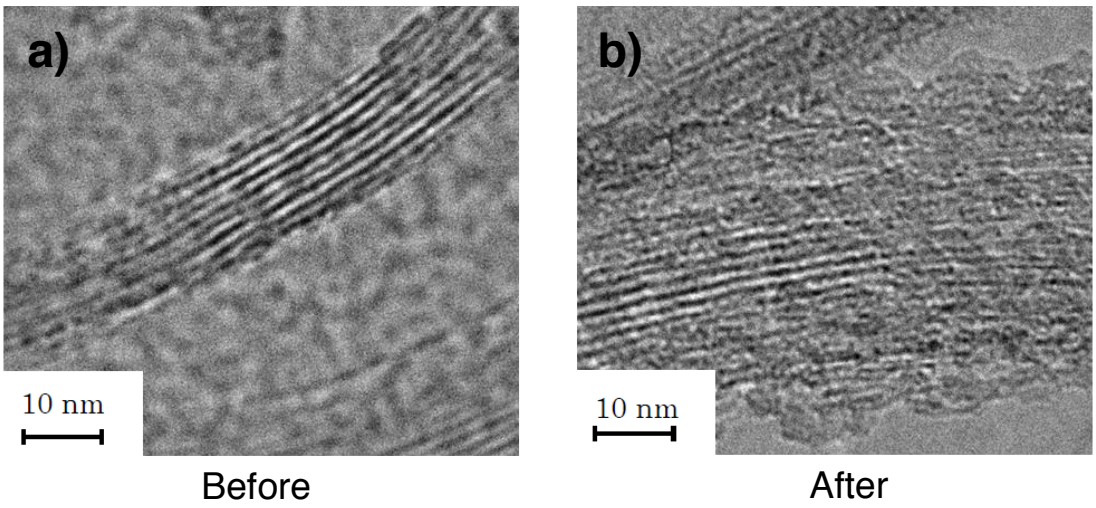


Figure 2. Deposition of MoS_2 on CNT before (a) and after (b)

In order to identify the deposition of MoS_2 on CNT, the surface of MoS_2 flakes on CNT bundles was analyzed by auger electron spectroscopy (AES). (Figure 3) Element compositions from the AES spectrum confirm the existence of MoS_2.

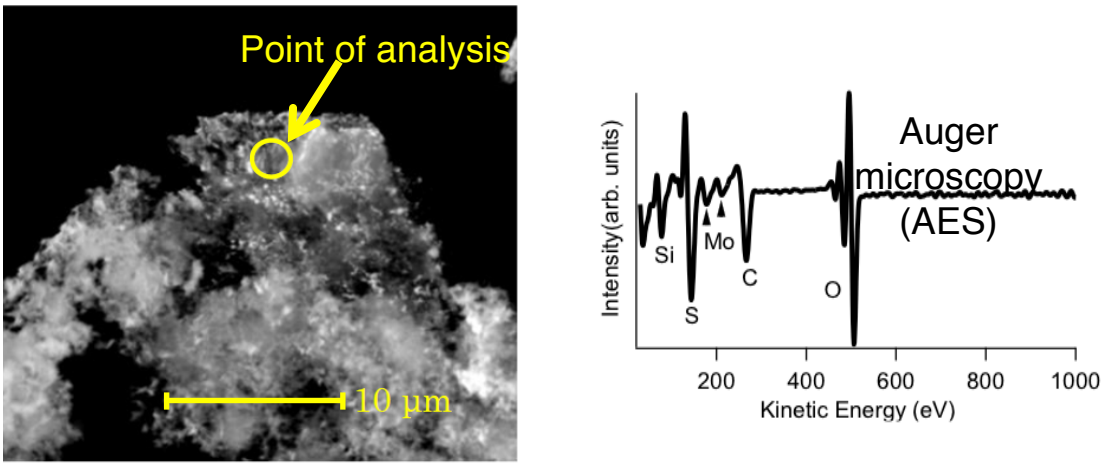


Figure 3. AES of a MoS_2 flake on a CNT bundle

To consolidate the formation of multilayer, Raman spectroscopy was carried out to analyze the thickness. Figure 4 shows Raman peaks of MoS_2 on CNT between 100 cm^{-1} and 600 cm^{-1}

of Raman shift. CNT's radial breathing mode (RBM) appeared at around 190cm^{-1} indicating the CNT bundles. The MoS_2 sheet deposited exhibits two Raman characteristic bands at 385.8 cm^{-1} and 403.8 cm^{-1} with the full-width-half-maximum values of 7.787 cm^{-1} and 8.370 cm^{-1}, corresponding to the out-of-plane A_{1g} and in-plain E^1_{2g} modes each. Note that the peak frequency difference between A_{1g} and E^1_{2g} modes (Δ) can be used to identify the layer number of MoS_2. The value of Δ, 0.583 cm^{-1} reveals that the multilayer of MoS_2 has been successfully deposited. [34]

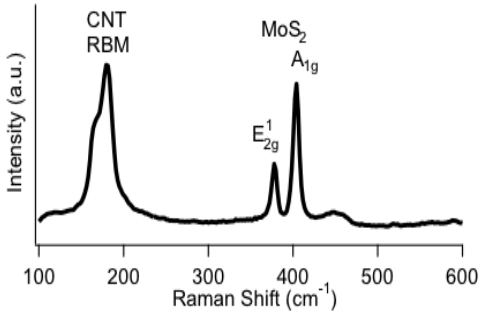


Figure 4. Raman spectrum of multilayered MoS_2 on CNT bundles

Next, we fabricated an OSC device using MoS_2 on CNT as electron acceptor and charge transporting material, respectively. 3 wt% of MoS_2CNT flakes in ODCB is thoroughly mixed in a P3HT solution before spin coating it on a ZnO film at 850 rpm for 45 seconds. Interaction between P3HT and MoS_2 CNT has been evidenced by our UV-Vis spectroscopy. (Figure 5) Figure 5a shows a typical P3HT spectrum. Figure 5b shows a spectrum where enhancements in shoulders at 450 nm^{-1}, 580 nm^{-1}, and 650 nm^{-1} confirm the existence of MoS_2. [35] In addition, the strong absorption peak at 610 nm and broadening of the spectrum indicates a high degree of structural order in the active layer in support of π-π interactions between CNT and P3HT.[36] (Figure 6) Nonetheless, we are still not sure of the reason why we cannot observe SWCNT peaks around 1000 nm^{-1}. We suspect two reasons here: one is that the intensity of SWCNT peaks are intrinsically much weaker than MoS_2 absorption and the amount of SWCNT we used in here is too little for the detection. Second reason is that the SWCNT purchased from Hipco typically does not show absorption peaks around 1000 nm,

which could be due to the broad range of SWCNT diameters and impure nature of the product.[37, 38]

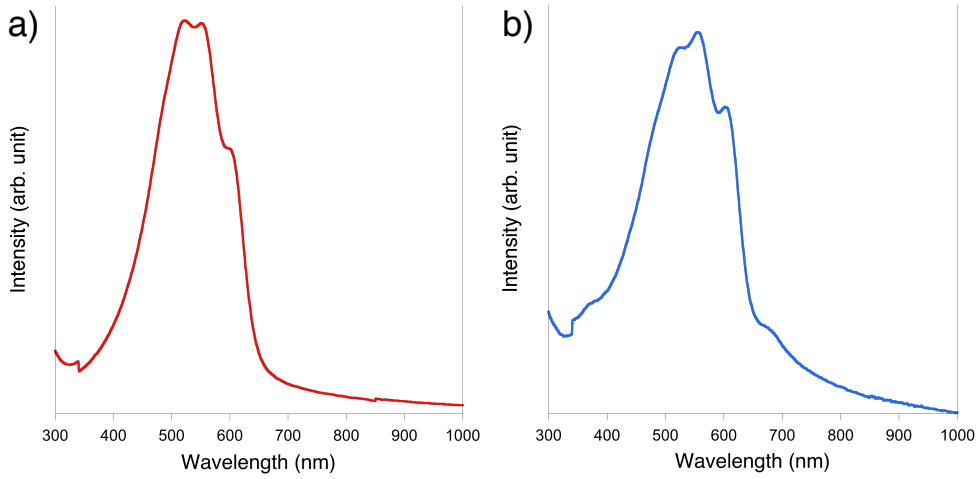


Figure 5. UV-Vis spectra of a) P3HT film and b) P3HT mixed with MoS_2CNT (3 wt%)

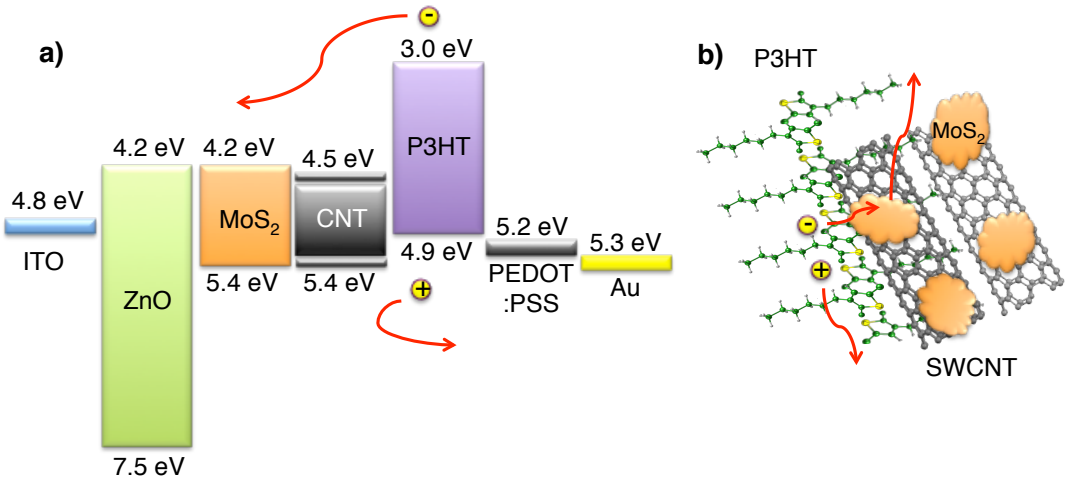


Figure 6. a) Energy band alignment of an P3HT:MoS_2CNT solar cell where CNT is semiconducting and metallic mixed. Metallic CNT exhibits workfunction of 4.5-5.0 eV b) graphical illustration of P3HT:MoS_2CNT photoactive layer

To assess the impact of the MoS_2 as electron acceptor, we performed PL measurement on both MoS_2CNT/P3HT solution and film. The excitation wavelength is 400 nm as derived from the UV-Vis spectrum. For the solution samples, we cannot observe anything. It could be the ODCB solvent used hindering the measurement and interaction between the two species or the concentration of the solution is not adequate. However, for the film samples where MoS_2CNT and P3HT have been mixed in different ratios show PL quenching specifically, from the sample, where 2.8 wt% of MoS_2CNT to P3HT, has been used. The quenching is further enhanced with the increase in MoS_2CNT composition to 3 wt%. Using higher concentration of MoS_2CNT does not quench the PL spectrum completely but rather reverts back to non-quenched spectrum. This suggests that the presence of MoS_2CNT induces the dissociation of excitons generated in the polymer and 3 wt% is the most optimized concentration. (Figure 7)

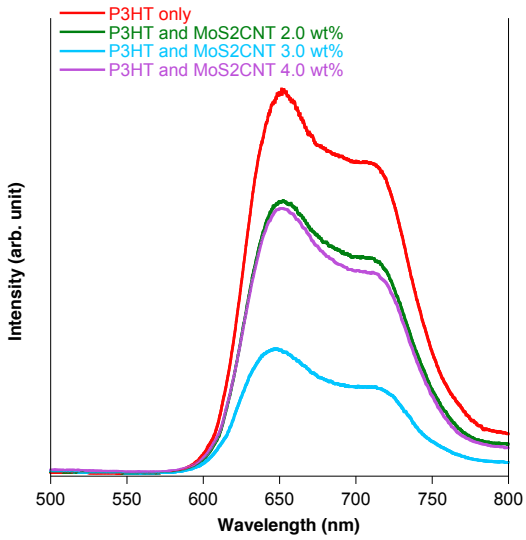


Figure 7. Photoluminescence data of the active layer with increase in MoS_2CNT concentration

Finally, we show the device performance. The PCE, η of MoS_2CNT and P3HT mixture device is measured to be 0.46%, while both the reference samples of pristine SWCNT without MoS_2 deposition and P3HT alone devices give η = 0% and η = 0% each. (Figure 8, Table 1)

Significant increase in Voc, Jsc, and Rsh shows that MoS_2CNT functions as electron acceptor. However, rise in Rs and limited FF suggest that many undermining factors like a random orientation of MoS_2CNT, small coverage of MoS_2 nanoflakes on CNT, purity of SWCNT, and thickness of SWCNT may have hampered the device potential. We also attribute to MoS_2CNT coverage and CNT's surface to volume ratio for the limited performance.

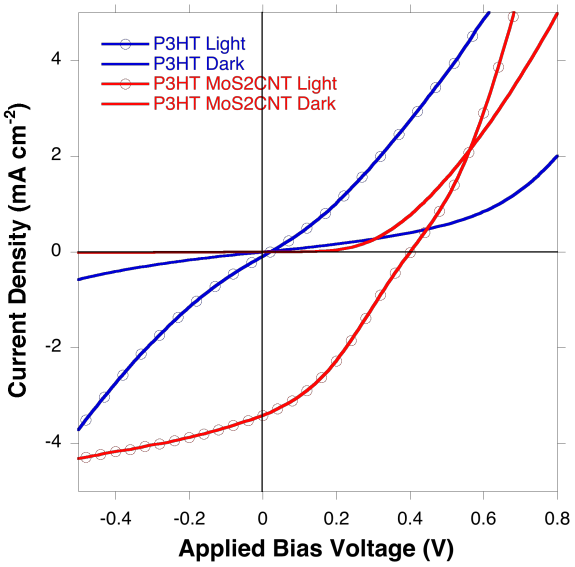


Figure 8. J-V curve of the P3HT only solar cell and P3HT:MoS_2CNT solar cell

Active Layer	V_{OC} (V)	J_{SC} (mA/cm^2)	FF	R_s(Ωcm^2)	R_{sh}(Ωcm^2)	PCE (%)
P3HT (ref.)	0.19	0.09	0.29	15.5	1.53E+01	0.01
P3HT/CNT	0.12	0.04	0.25	187	1.54E+03	0.00
P3HT/MoS_2CNT	0.40	3.42	0.33	43.6	3.77E+03	0.46

Table 1. Photovoltaic parameters of P3HT device, P3HT:CNT device, and P3HT:MoS_2CNT device

4. Conclusion

We have demonstrated an OSC where MoS_2 forms a BHJ and function as electron acceptor species by depositing multilayer on unpurified SWCNT bundles. Despite many advantages of multilayered MoS_2, application in OSC had been limited due to its immiscibility with P3HT. Our inverted OSC employing the MoS_2CNT:P3HT leads to the efficiency of 0.46%, which is

respectable considering the fact that the expensive purely semiconducting SWCNT:P3HT inverted OSC has given 0.72%. We hope this finding can provide guidance to other researchers working on the next-generation MoS_2 based photovoltaic device.

Reference

[1] W. Huynh, J.J. Dittmer, A.P. Alivisatos, Science 295 (2002) 2425.

[2] A. Splendiani, L. Sun, Y. Zhang, T. Li, J. Kim, C.Y. Chim, G. Galli, F. Wang, Nano Lett. 10 (2010) 1271.

[3] K.K. Liu, W. Zhang, Y.H. Lee, Y.C. Lin, M.T. Chang, C.Y. Su, C.S. Chang, H. Li, Y. Shi, H. Zhang, C.S. Lai, L.J. Li, Nano Lett. 12 (2012) 1538.

[4] K.F. Mak, C. Lee, J. Hone, J. Shan, T.F. Heinz, Phys. Rev. Lett. 105 (2010) 136805.

[5] S. Najmaei, Z. Liu, P.M. Ajayan, J. Lou, Appl. Phys. Lett. 100 (2010) 013106.

[6] D.J. Li, U.N. Maiti, J. Lim, D.S. Choi, W.J. Lee, Y. Oh, G.Y. Lee, and S.O. Kim, Nano Lett. 14 (2014) 1228.

[7] B.G. Streetman, Solid State Electronic Devices, Chapt. 3, Prentice Hall, Upper Saddle River, NJ, 1995.

[8] V.I. Arkhipov, P. Heremans, E.V. Emelianova, G.J. Adriaenssens, H. Bässler, Appl. Phys. Lett. 82 (2003) 3245.

[9] R.H. Friend, R.W. Gymer, A.B. Holmes, J.H. Burroughes, R.N. Marks, C. Taliani, D.D.C. Bradley, D.A. Dos Santos, J.L. Brédas, M. Lögdlund, W.R. Salaneck, Nature 397 (1999) 121.

[10] Q.H. Wang, K. Kalantar-Zadeh, A. Kis, J.N. Coleman, M.S. Strano, Nat. Nanotechnol. 7 (2012) 699.

[11] T. Shimada, F.S. Ohuchi, B.A. Parkinson, Jpn. J. Appl. Phys. 33 (1994) 2696.

[12] T. Fujimori, A. Morelos-Gomez, Z. Zhu, H. Muramatsu, R. Futamura, K. Urita, M. Terrones, T. Hayashi, M. Endo, S.Y. Hong, Y.C. Choi, D. Tomanek, K. Kaneko, Nat. Comm. 4 (2013) 2162.

[13] R. Fivaz, E. Mooser, Phys. Rev. 163 (1967) 743.

[14] K. Takanezawa, K. Tajima, K. Hashimoto, Appl. Phys. Lett. 93 (2008) 063308.

[15] A.M. Peiro, P. Ravirajan, K. Govender, D.S. Boyle, P. O'Brien, D.D.C. Bradley, J. Nelson, J.R. Durant J. Mater. Chem. 16 (2006) 2088.

[16] D.C. Olson, S.E. Shaheen, R.T. Collins, D.S. Ginley, J. Phys. Chem. C 111 (2007) 16670.

[17] K.M. Coakley, M.D. McGehee, Appl. Phys. Lett. 83 (2003) 3380.

[18] Y. Yoon, K. Ganapathi, S. Salahuddin, Nano Lett. 11 (2011) 3768.

[19] B. Radisavljevic, A. Radenovic, J. Brivio, V. Giacometti, A. Kis, Nat. Nanotechnol. 6 (2011) 147.

[20] Y. Zhang, J. Ye, Y. Matsuhashi, Y. Iwasa, Nano Lett. 12 (2012) 1136.

[21] H. Qiu, L. Pan, Z. Yao, J. Li, Y. Shi, X. Wang, Appl. Phys. Lett. 100 (2012) 123104.

[22] H. Hwang, H. Kim, J. Cho, Nano Lett. 11 (2011) 4826.

[23] M. Shanmugam, T. Bansal, C.A. Durcan, B. Yu, Appl. Phys. Lett. 100 (2012) 153901.

[24] Y.H. Lee, X.Q. Zhang, W. Zhang, M.T. Chang, C.T. Lin, K.D. Chang, Y.C. Yu, J.T.W. Wang, C.S. Chang, L.J. Li, T.W. Lin, Adv. Mater. 24 (2012) 2320.

[25] Y. Li, H. Wang, L. Xie, Y. Liang, G. Hong, H. Dai, J. Am. Chem. Soc. 133 (2011) 7296.

[26] F.K. Perkins, A.L. Friedman, E. Cobas, P.M. Campbell, G.G. Jernigan, B.T. Jonker Nano Lett. 13 (2013) 668.

[27] A.M.V.D. Zande, P.Y. Huang, D.A. Chenet, T.C. Berkelbach, Y.M. You, Nat. Mater. 12 (2013) 554.

[28] M.S. Arnold, J.D. Zimmerman, C.K. Renshaw, X. Xu, R.R. Lunt, C.M. Austin, S.R. Forrest Nano Lett. 9 (2009) 3354.

[29] Z. He, C. Zhong, S. Su, M. Xu, H. Wu, Y. Cao, Nat. Photonics 6, (2012) 591.

[30] S. Ren, M. Bernardi, R.R. Lunt, V. Bulovic, J.C. Grossman, S. Gradečak, Nano Lett. 11 (2011) 5316.

[31] A.K.K. Kyaw, D.H. Wang, V. Gupta, J. Zhang, S. Chand, G.C. Bazan, A.J. Heeger, Adv. Mater. 25 (2013) 2397.

[32] C. Roxlo, R. Chianelli, H. Deckman, A. Ruppert, P. Wong, J. Vac. Sci. Technol. A 5 (1987) 555.

[33] T. Li, G. Galli, J. Phys. Chem. C 111 (2007) 16192.

[34] H. Li, Z.Y. Yin, Q.Y. He, H. Li, X. Huang, G.Lu, D.W.H. Fam, A.I.Y. Tok, Q. Zhang, H. Zhang, Small 8 (2012) 63.

[35] X. Gu, W. Cui, H. Li, Z. Wu, Z. Zeng, S.T. Lee, H. Zhang, B. Su Adv. Energy Mater. 3 (2013) 1262.

[36] P.J. Brown, D.S. Thomas, A. Kohler, J.S. Wilson, J.S. Kim, C.M. Ramsdale, H. Sirringhaus, R.H. Friend, Phys. Rev. B 67 (2003) 064203.

[37] X. Zhang, Z. Yu, C. Wang, D. Zarrouk, J.T. Seo, J.C. Cheng, A.D. Buchan, K. Takei, Y. Zhao, J.W. Ager, J. Zhang, M. Hettick, M.C. Hersam, A.P. Pisano, R.S. Fearing, A. Javey, Nat. Commun. 5 (2014) 2983.

[38] J.L. Bahr, J.M. Tour, J. Mater. Chem. 12 (2002) 1952.